Semi-annual Report
July - December 1997

Michael D. King and Si-Chee Tsay
Goddard Space Flight Center
Greenbelt, MD 20771

Abstract

Our major achievements of the past six months were: (i) the successful delivery of the MOD_PR06OD *V2* algorithm, (ii) the revision (version 5) of ATBD-MOD-05/06 Cloud Product, and (iii) the overall analysis of SCAR-B and other observational data for various publications.

I. Task Objectives

With the use of related airborne instrumentation, such as the MODIS Airborne Simulator (MAS) and Cloud Absorption Radiometer (CAR) in intensive field experiments, our primary objective is to extend and expand algorithms for retrieving the optical thickness and effective radius of clouds from radiation measurements to be obtained from the Moderate Resolution Imaging Spectroradiometer (MODIS). The secondary objective is to obtain an enhanced knowledge of surface angular and spectral properties that can be inferred from airborne directional radiance measurements.

II. Work Accomplished

a. MODIS-related Algorithm Study

The cloud retrieval algorithm, MOD06OD version 2 package, was delivered to SDST in early September using the MODIS electronic code delivery system. The package includes MOD06OD version 2 source code and the supporting system items required by version 2 delivery. The communication with SSTG (Science Software Transfer Group) personnel confirmed that our delivered package was accepted by CMO (Configuration Manage Officer) and passed to SSTG for further review. While the structure of the code is complete, several subroutines and data files (notably, MOD28 and MOD43 processing packages for ancillary data, atmosphere correction, and QA) will be modified in a later update. Interfaces, including ECS metadata procedures and up-to-date L1B, L1A (geolocation) and cloud mask readers, were integrated into the package and a new HDF output procedure was re-written for MOD06OD, due to the new requirements of HDF-EOS and combining MOD06 products. The ancillary data flow chart was generated and its creating package was also integrated into the version 2 code and fully tested. The ancillary data processing package includes cloud heights (from MOD06), land temperature (from DAO and NCEP surface air temperature), ocean temperature (from DAO and NCEP), mean temperature above cloud (from MOD07, NCEP, DAO, and standard atmosphere), precipitable water above cloud (from MOD07, NCEP, DAO, and standard atmosphere), and surface albedo (from CERES/SARB map). Interfaces to read in the intermediate ancillary data were completed and integrated. Due to processing differences between the cloud retrieval (process one instrument scan at a time) and the ancillary data procedure (process one whole granule at a time), the code structure had to be modified and was completed.

In the atmospheric correction routine, the current delivery simply returns constant values of above-cloud atmospheric transmittance, while the final version will use a look-up table of precalculated transmittance values. Further sensitivity studies on the transmittance of the seven channels (applied by MOD06OD) will be conducted using the correlated-k distribution method. Look-up tables of one-way and two-way transmittance at different solar zenith angle, viewing angle, water vapor load, and cloud-top-pressure will be created for each of the seven channels by combining the correlated-k distribution calculations using several standard atmospheres. However, with the completed code structure in place, SDST has agreed to begin integration of the code. Development of the atmospheric correction subroutine and QA subroutine is ongoing.

The visible/near-IR thermodynamic phase (post-launch parameter) algorithm is also under development. The algorithm is expected to determine whether a cloud is made of ice or liquid water by comparing ratios of reflectances at several wavelengths as functions of solar zenith angle, viewing zenith angle, relative azimuthal angle, cloud optical thickness, and effective particle radius. Rather than performing new forward calculations of reflectances and asymptotic parameters of ice and water clouds, work is underway to adapt the MOD_PR06 code so that all needed reflectances can be interpolated from the ice/water cloud libraries, with appropriate corrections for Rayleigh scattering in the 0.66 µm channel and emission in the 3.7 µm channel. After a thorough theoretical study of ice/water cloud reflectances, an operational algorithm will be developed and tested using data acquired by MAS during three campaigns (ARMCAS, SUCCESS, and TARFOX) where both ice and water clouds were observed.

We have completed and delivered code to perform space-time aggregation of MODIS atmosphere products; i.e. code to produce Level-3 daily gridded files from a collection of Level-2 granules. This code will be used to aggregate all products (aerosol over land, aerosol over ocean, water vapor, clouds, and atmospheric profiles) for the Atmosphere group. A significant design change was made to add several (in some cases, as many as 25) local attributes to each Scientific Data Set (SDS) in the Level-3 file specification, and use the values in the Level-3 file to control the processing of each parameter. Although this has caused a significant delay, we believe the code will be substantially more robust and flexible. The local attributes serve several functions. First, they control which statistics are produced, by indicating that the output SDS is derived from the input values through simple spatial averaging. Other local attributes may hold the ancillary information needed to compute certain statistics (e.g., the bin boundaries to be used when histograms are computed). In addition, the attributes help to document the processing path taken at run time. Most parameters, for example, make use of a Quality Assurance value that is stored as a bit string in a byte array in the Level-2 granule. These QA values are used to exclude some observations from the daily averages. The specification of which bits from which byte array are now determined by local attributes in the Level-3 file, so that users of the daily averages will know exactly how they have been computed. Finally, the output files are now guaranteed to be consistent with the file specification. Changes to the desired output, therefore, can be performed simply by changing the file specification. Various MOD products with prescribed means and standard deviations were created as synthetic data to check the flow of the Level-3 processing packages and to find any bugs.

Code for MOD_PR08T, the MODIS Level-3 Daily Integrated Atmosphere Zonal Tile process, was delivered and accepted in November. The code constitutes 12,000 lines of Fortran 90 code, and has been tested using synthetic MODIS data. After discussions with ECS, the code was modified so that it could be run in parallel. As a result of these discussions, the statistics for each daily zonal tile (5 degrees of latitude by 360 degrees of longitude) are computed and written to a separate file. These zonal files are not archived, but are used as input to process MOD_PR08D, which reads each zonal tile file and builds a composite daily global file. The design for process MOD_PR08D has been completed. It is worth noting that approximately 3500 lines of code developed for MOD_PR08T are also used in MOD_PR08D and MOD_PR08M, the processes for computing monthly averages. This code reuse significantly shortened development times for the latter two processes. Some of this code is used for routine operations on HDF files; this code has been placed on the World Wide Web for public use.

b. MODIS-related Instrumental Research

During vicarious calibration of the CAR UV-channel, we discovered that there was a manufacturing flaw in the UV filter—a spurious transmission at ~365 nm. This flaw caused at least 2/3 of the signal to be from outside the designed spectral bandwidth specifications. Thus, UV-B data gathered during the MAST, ARMCAS, SCAR-B, and TARFOX experiments are contaminated by UV-A radiation. In working with optics engineers in Code 924, we plan to replace the old UV-channel with two narrowband filters (FWHM no more than 5 nm) at least 40 nm apart. We prefer the 340 and 380 nm bands, based on the fact that reflectances at both channels are already well known from nearly 20 years of TOMS and SBUV measurements.

To prepare the CAR for the FIRE-III Arctic campaign in May 1998, we plan to do a thorough calibration and characterization of the CAR in April, after the University of Washington has finished integrating the CAR on their new CV-580 research aircraft. To determine if the CAR has a polarization sensitivity in any of its channels, we have ordered a 5.5-inch wide polarizer that is large enough to cover the CAR's entire field of view. In addition, to replace the current defective UV filter, we have also ordered new UV filters with transmissions of at least 60% at 380 nm. If the new supporting equipment (monochromator, new brighter lamp source, etc.) are functional, we plan to make thorough determinations of stray-light errors, visible-light contamination of the UV-channel, and total spectral throughput of all channels up to 1.7 µm, sometime in April. We have measured transmissions of three duplicate components in the UV optical path: a UV lens, and two dichroics designed to be highly reflective for UV-B. While the transmission of the UV lens appears to be constant through both UV-B and UV-A (~80%), the two dichroics, which are highly reflective in the UV-B, have transmissions of ~35% and ~75% at 380 nm. Nevertheless, assuming that at least 2/3 of the signal from the previous defective filter came from a spurious 5% transmission at 365 nm, it is estimated that the signal obtained by the CAR-UV channel during FIRE-III will be roughly twice as strong as the signal from the defective UV filter. In addition, all known spare optical, mechanical, and electronic parts and original schematic diagrams of the CAR have now been inventoried and gathered in one large filing cabinet.

c. MODIS-related Services

Meetings

1. Michael King and Peter Soulen attended the *Third International Airborne Remote Sensing Conference and Exhibition*, held in Copenhagen, Denmark, on July 7-10, 1997, and presented papers "MODIS Airborne Simulator: Radiative properties of smoke and clouds during ARMCAS and SCAR-B" and "Cloud Absorption Radiometer: Airborne measurements of clouds and surface reflectance," respectively.

2. Si-Chee Tsay attended the *IAMAS Symposium on Radiative Forcing and Climate*, held in Melbourne, Australia, on July 1-9, 1997, chaired a session on "*Radiative Forcing by Aerosol,*" and presented a paper on "Sensitivity analysis of cloud forcing in the Arctic."

3. Si-Chee Tsay attended the *IGARSS'97 Remote Sensing—A Scientific Vision for Sustainable Development*, held in Singapore, on August 3-8, 1997, and presented a paper on "Global monitoring and retrievals of atmospheric aerosols and clouds."

4. Michael King and Si-Chee Tsay attended the *CERES Science Team meeting*, held in Corvallis, OR, on September 16-18, 1997, and presented a paper on "Cloud mask and cloud properties retrieval in the Arctic: ARMCAS results."

5. Steve Platnick and Michael King regularly attended weekly MODIS Technical Team meetings. Steve Platnick participated in MCST reflectance solar calibration issues, especially those effecting the SWIR bands. This includes analyzing the impact of the recently discovered 2.5 and 5.3 µm light leakage prob-

lem.

6. Michael King attended the *Earth Observation and Environmental Information* conference, held in Alexandria, Egypt, on October 13-16, 1997, and presented a paper on "Airborne measurements of surface anisotropy."

7. Michael King, Steve Platnick, Ran Song and Si-Chee Tsay attended the *MODIS Science Team meeting*, held in College Park Holiday Inn, MD, on October 22-24, 1997 to discuss MODIS algorithm delivery and products.

8. Si-Chee Tsay attended the *AGU Fall Meeting*, held in San Francisco, CA, on 8-12 December 1997, and presented a paper on "Determination of Aerosol Humidification Factors from SCAR-B and TARFOX Ground-based Measurements," at the TARFOX session.

Seminars

1. Tsay, S. C., "Global Monitoring and Retrievals of Atmospheric Aerosols and Clouds," at the Center for Space Remote Sensing Research, National Central University, Taiwan, August 11, 1997.

2. Pincus, R., "Clouds, Radiation and Climate" at San Francisco University High School, San Francisco, California, November, 1997.

III. Data/Analysis/Interpretation

a. Data Processing

All recent MAS 50-channel flights have been processed to level-1B (calibrated and geolocated radiances) using final radiometric and spectral calibration, with data sent to the Goddard or Langley DAAC (Distributed Active Archive Center, cf. Web site below). These data sets are ARMCAS (June 1995, 9 flights), SCAR-B (August-September 1995, 12 flights), SUCCESS (April-May 1996, 18 flights), TARFOX (July 1996, 10 flights), and WINCE (January-February 1997, 10 flights). In addition, browse images, a MAS data user's guide, software for unpacking and interpreting the data, and information on where and how to obtain data, are also accessible via World Wide Web (http://ltpwww.gsfc.nasa.gov/MAS).

b. Analysis and Interpretation

Multispectral images of the reflection function and brightness temperature in 10 distinct bands of the MAS, acquired in SCAR-B, were used to derive a confidence in clear sky (or alternatively the probability of cloud), shadow, fire, and heavy aerosol, as shown in Figs. 1 and 2. In addition to multispectral imagery, monostatic lidar data were obtained along the nadir ground track of the aircraft and used to assess the accuracy of the cloud mask results. Our comparisons between remote sensing-derived values of the heavy aerosol and fire mask and high resolution imagery and monostatic lidar measurements demonstrate that the aerosol mask properly detects heavy aerosol over land during daytime in Brazil, at least during the biomass burning season. As presently implemented, the heavy aerosol mask is not applied when the reflection function at 2.19 µm ($R_{2.19}$) exceeds 0.2. Hence, for deforested areas and urban/suburban environments, conditions for which $R_{2.19}$ is typically larger than 0.2, the heavy aerosol mask is not tested or applied. In the optically thinner regions of the MAS scene, heavy aerosol is more likely to be detected off nadir than at nadir, due largely to

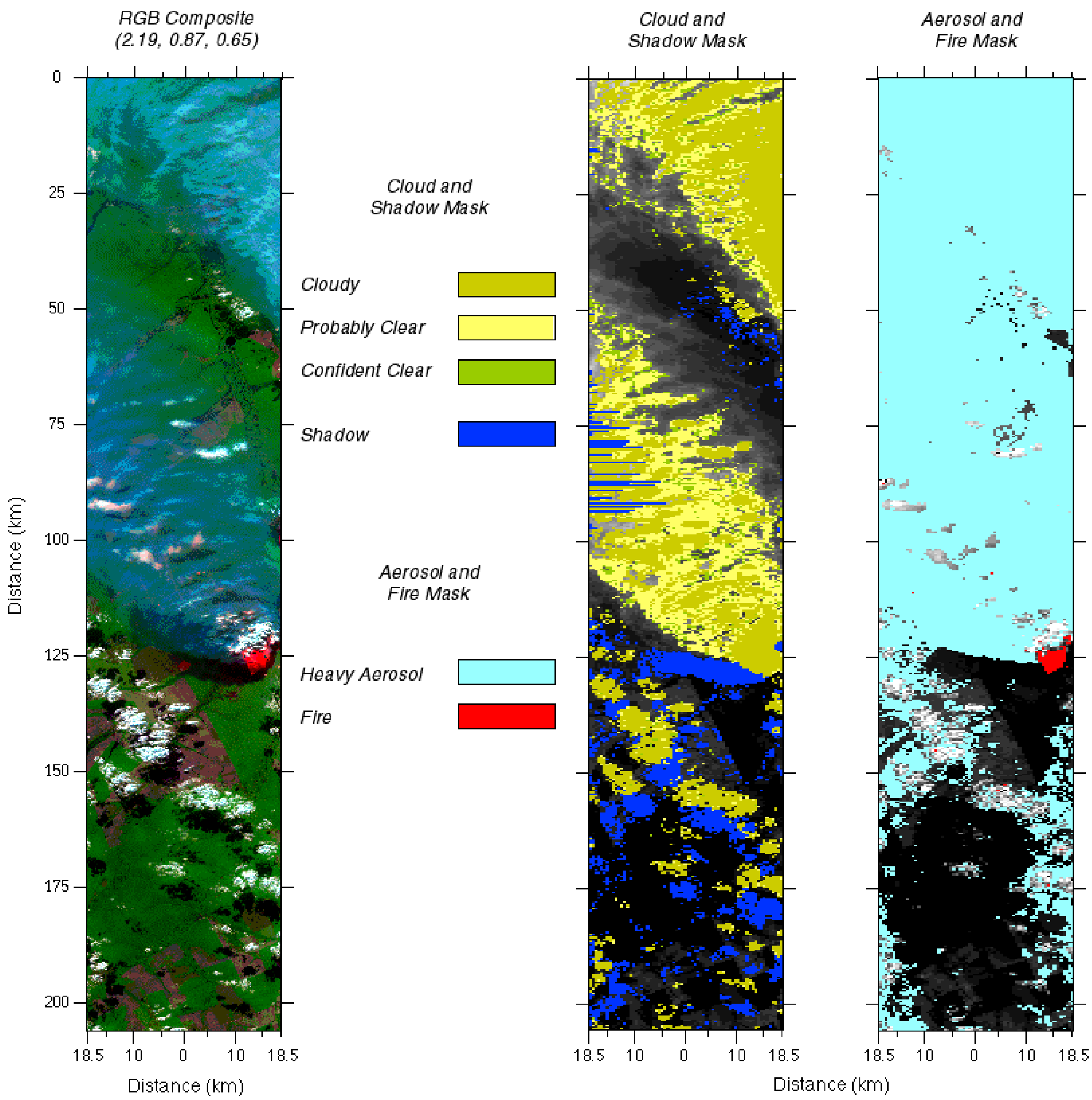

Figure 1. Composite image (left) of smoke, burn scars, and unburned vegetation in Mato Grosso on August 23, 1995. The RGB assignment is red (2.19 µm), green (0.87 µm) and blue (0.65 µm), and is based on the individual channels shown in Fig. 5. The middle panel is the resultant cloud and shadow mask, and the final panel the heavy aerosol and fire mask. Most of the scene is classified as heavy aerosol, as expected. The background image on which the cloud and aerosol mask are overlaid is the MAS reflectance image at 0.65 µm.

the fact that the heavy aerosol thresholds are not view-angle dependent, as they should be. At least for the spatial resolution of MAS (50 m at nadir), it is extremely easy to detect hot fires due to their strong thermal contrast to their surroundings. In our application of the fire mask, we used the 3.74 and 11.02 µm bands of MAS, though we could have utilized the 2.19 or 3.90 µm bands.

The cloud mask also appears to work well in Brazil, except under extremely thick aerosol conditions for which the reflection function at 0.87 µm ($R_{0.87}$) exceeds our

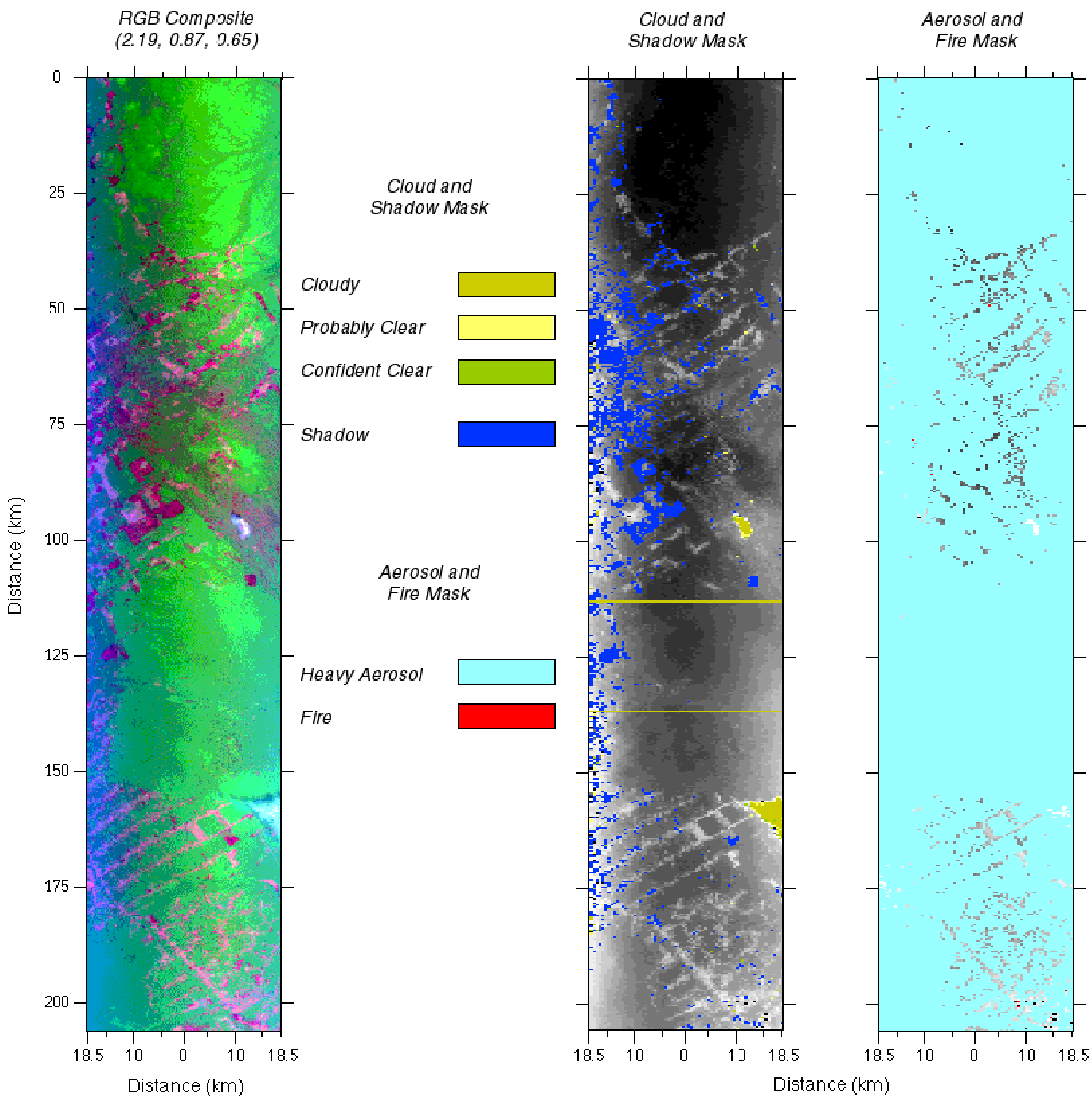

Figure 2. Composite image (left) of smoke, burns, and unburned vegetation in Mato Grosso on September 4, 1995. The RGB assignment is red (2.19 µm), green (0.87 µm) and blue (0.65 µm), and is based on the individual channels shown in Fig. 9. The middle panel is the resultant cloud and shadow mask, and the final panel the fire and heavy aerosol mask. Most of the scene is classified as heavy aerosol, as expected, with only a few clouds. The background image on which the cloud and aerosol mask are overlaid is the MAS reflectance image at 0.65 µm.

expectations for aerosol scattering. Under these optically thick conditions, the thickest part of the aerosol layer is misidentified as cloud ('fumulus'). The isolated cumulus mediocris clouds and the fire-induced cumulus congenitus clouds appear to be properly identified as cloud. Furthermore, our results for the shadow mask appear to work best for cloud shadows on the ground, and not very well for shadows of upper clouds on lower clouds. Areas where the shadow mask has its greatest difficulties are burn scars, which are naturally quite dark, especially in the forward scattering direction. This analysis shows that the cloud and aerosol mask being developed for operational use on MODIS, and tested using MAS data in Brazil, is quite capable of separating cloud, aerosol, shadow and fires during daytime conditions over land.

Three types of surface spectral anisotropy (i.e., cerrado, dense forest, and heavy smoke over dense forest; photographs shown in Fig. 3) measured by the CAR during SCAR-B were analyzed and submitted for publication. Based on analysis of these measurements, results show distinct spectral characteristics for various types of surfaces. The spectral anisotropy of cerrado, dense forest, and heavy smoke over dense forest, shown respectively in Figs. 4-6, revealed fairly symmetric patterns around the principal plane, with varying strengths and angular widths of the hot spot (backscattering peak in the anti-solar direction). In the shortwave-infrared region, the aerosol effect is suppressed and these hot spots are clearly seen in the bidirectional reflectance of the smoke layer over dense forest. In the 0.869-1.271 µm range, the shape of the hot spot is spiky; while the strength is reduced and becomes broader towards longer (e.g., 1.643 and 2.207 µm) and shorter (e.g., 0.472 and 0.675 µm) wavelengths, where chlorophyll absorption prevails. A secondary peak in the backscattering direction exists near 75° for the 0.869-1.271 µm range over cerrado and dense forest (but not for the smoke layer), and diminished for the 0.675, 1.643, and 2.207 µm channels. This phenomenon may be related to multiple scattering among leaves with particular leaf angle distributions.

These detailed measurements of the angular distribution of spectral reflectance have been used to compute surface albedo, as listed in Table 1. Large discrepancies are found between these spectral albedos and those of the measured nadir reflectance. These angular and spectral dependencies can be utilized to retrieve either surface characteristics, using a few independent parameters, or aerosol microphysical and optical properties (e.g., size distribution and single-scattering parameters), if proper physical and radiation models are used. The CAR measurements, combined with the boundary layer aircraft measurements of aerosol physical properties and radiosonde observations, form an unprecedented data set with many scientific results anticipated following more extensive radiative transfer modeling in the future.

(a)

(b)

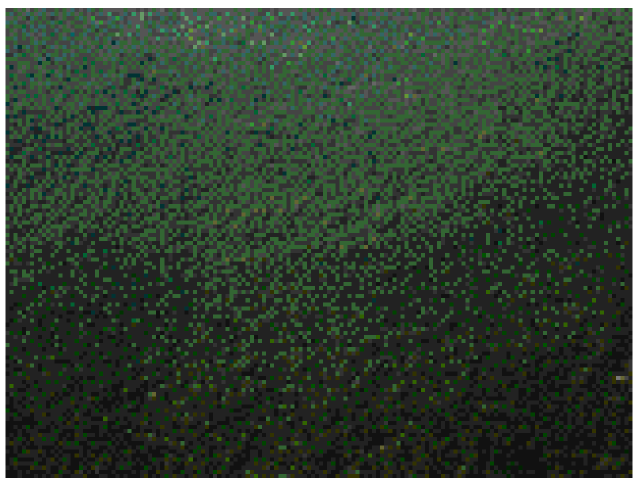

(c)

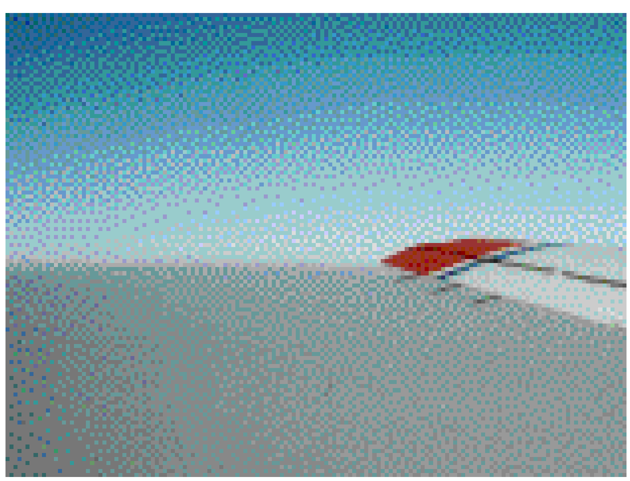

Figure 3 Photographs of (a) cerrado, (b) dense forest, and (c) smoke layer, taken during SCAR-B from the University of Washington C-131A aircraft.

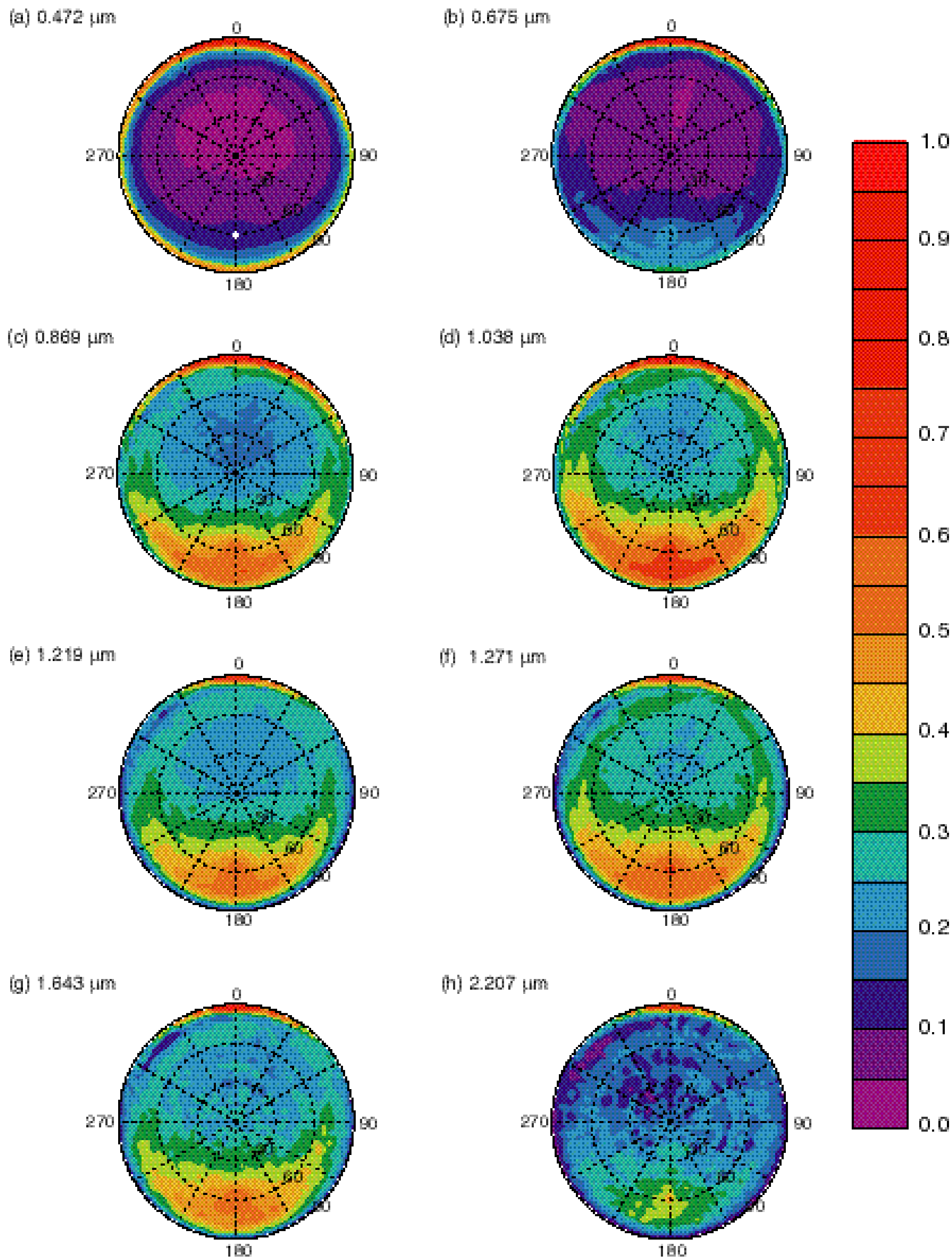

Figure 4. Spectral measurements of surface bidirectional reflectance over cerrado on August 18, 1995 during SCAR-B. The location of the anti-solar point at θ = 60° and φ = 180° is indicated in (a).

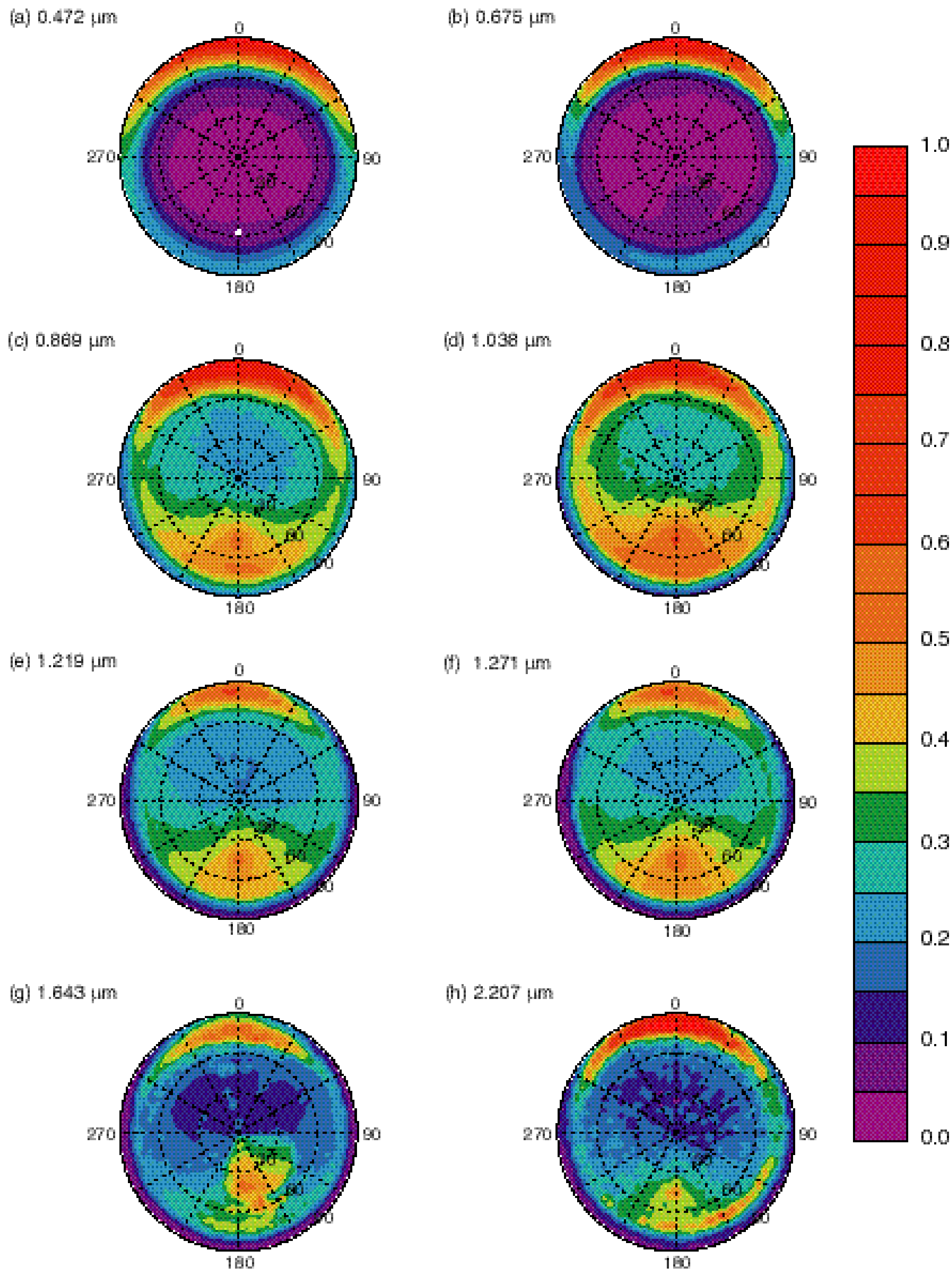

Figure 5. Spectral measurements of surface bidirectional reflectance over dense forest (large canopy type) on August 25, 1995 during SCAR-B. Note that the BRF of 2.207 μm was doubled for showing better contrast.

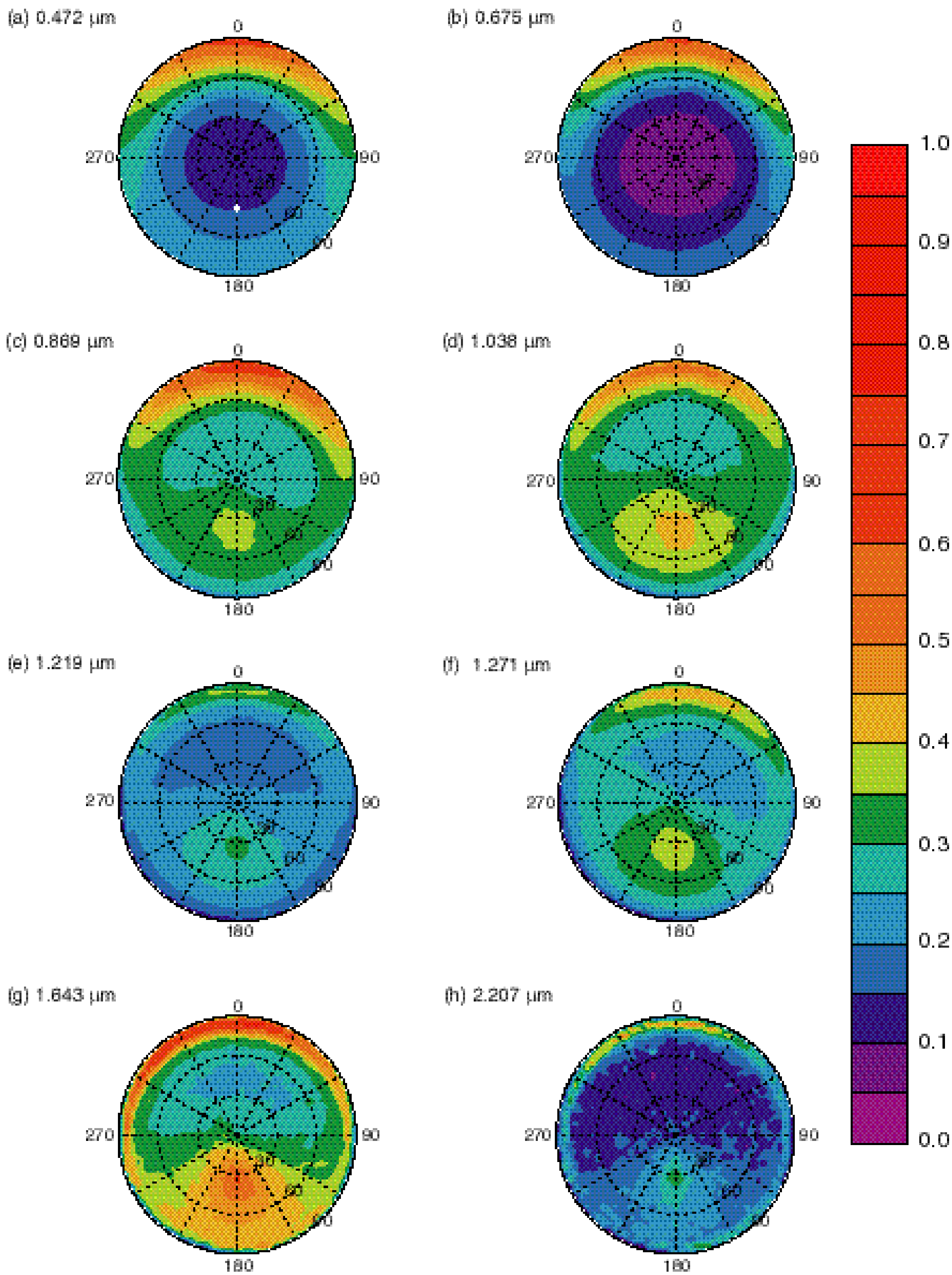

Figure 6. Spectral measurements of surface bidirectional reflectance above smoke layer (over dense forest) on September 6, 1995 during SCAR-B. Note that the BRFs of 1.643 and 2.207 µm were doubled for showing better contrast.

Table 1. Computed spectral albedo and measured nadir reflectance for (a) cerrado, (b) dense forest, and (c) thick smoke layer over forest.

Central wavelength (μm)	Bandwidth (μm)	Solar flux ($Wm^{-2}μm^{-1}$)	Solar zenith angle	Albedo	Nadir reflectance
(a) Cerrado (August 18, 1995)					
0.472	0.021	1974.4	59.07° - 61.73°	0.075 ± 0.0022	0.042 ± 0.0067
0.675	0.020	1480.4	59.07° - 61.73°	0.096 ± 0.0030	0.072 ± 0.0202
0.869	0.020	949.13	59.07° - 61.73°	0.271 ± 0.0031	0.209 ± 0.0327
1.038	0.020	675.07	59.07° - 61.73°	0.319 ± 0.0047	0.250 ± 0.0393
1.219	0.020	477.86	59.07° - 61.73°	0.291 ± 0.0048	0.244 ± 0.0329
1.271	0.021	433.33	59.07° - 61.73°	0.319 ± 0.0059	0.270 ± 0.0367
1.643	0.041	230.99	59.63° - 60.71°	0.289	0.245 ± 0.0394
2.207	0.040	72.672	61.22° - 61.73°	0.202	0.179 ± 0.0352
(b) Dense forest (August 25, 1995)					
0.472	0.021	1979.4	54.79° - 58.56°	0.083 ± 0.0073	0.021 ± 0.0046
0.675	0.020	1484.1	54.79° - 58.56°	0.072 ± 0.0060	0.024 ± 0.0143
0.869	0.020	951.55	54.79° - 58.56°	0.317 ± 0.0149	0.240 ± 0.0370
1.038	0.020	676.79	54.79° - 58.56°	0.360 ± 0.0076	0.280 ± 0.0354
1.219	0.020	479.07	54.79° - 58.56°	0.285 ± 0.0046	0.232 ± 0.0338
1.271	0.021	434.43	54.79° - 58.56°	0.305 ± 0.0056	0.252 ± 0.0373
1.643	0.041	231.57	54.79° - 55.87°	0.221	0.184 ± 0.0727
2.207	0.040	72.857	56.96° - 58.56°	0.107	0.080 ± 0.0206
(c) Smoke layer (September 6, 1995)					
0.472	0.021	1989.8	39.14° - 36.36°	0.191 ± 0.0023	0.109 ± 0.0023
0.675	0.020	1491.9	39.14° - 36.36°	0.133 ± 0.0020	0.067 ± 0.0044
0.869	0.020	956.55	39.14° - 36.36°	0.313 ± 0.0017	0.288 ± 0.0130
1.038	0.020	680.34	39.14° - 36.36°	0.328 ± 0.0026	0.317 ± 0.0173
1.219	0.020	481.59	39.14° - 36.36°	0.223 ± 0.0021	0.224 ± 0.0114
1.271	0.021	436.72	39.14° - 36.36°	0.278 ± 0.0027	0.278 ± 0.0145
1.643	0.041	232.79	39.14° - 38.05°	0.171	0.160 ± 0.0101
2.207	0.040	73.240	37.49° - 36.36°	0.082	0.080 ± 0.0121

IV. Anticipated Future Actions

a. Continue to test and refine our delivered MODIS *v2* cloud retrieval algorithm, including the cloud mask interface, ice/water cloud libraries/logic tree, thermodynamic phase, and QA flags;

b. Continue to analyze MAS, AVIRIS, and CLS data gathered during the ARMCAS campaign, as well as AVHRR, University of Washington C-131A in situ data, and surface data, all with the express purpose of helping to develop the MODIS cloud masking algorithm;

c. Continue to analyze MAS, AVIRIS, and CLS data gathered during the SCAR-B and TARFOX campaigns, as well as University of Washington C-131A in situ and radiation data to study aerosol mask and aerosol-cloud interactions;

d. Continue to analyze surface bidirectional reflectance measurements obtained by the CAR during the Kuwait Oil Fire, LEADEX, ASTEX, SCAR-A ARMCAS, SCAR-B, and TARFOX experiments;

e. Attend the FIRE Arctic Cloud (January 28-30) working group meeting, to be held at NCAR, Boulder, CO, for the upcoming field campaign (May-June, 1998 in Alaska);

f. Attend the MODIS Atmosphere Group Retreat (February 3-5), to be held at St. Michaels Harbour Inn, for MODIS products.

V. Problems/Corrective Actions

No problems that we are aware of at this time.

VI. Publications

1. Ackerman, S. A., C. C. Moeller, K. I. Strabala, H. E. Gerber, L. E. Gumley, W. P. Menzel and S. C. Tsay, 1998: An infrared retrieval algorithm for determining the effective microphysical properties of clouds. *Geophys. Res. Lett*., in press.

2. Gao, B. C., W. Han, S. C. Tsay and N. F. Larsen, 1997: Cloud detection over arctic region using airborne imaging spectrometer data. *J. Appl. Meteor*., in press.

3. Kaufman, Y. J., P. V. Hobbs, V. W. J. H. Kirchhoff, P. Artaxo, L. A. Remer, B. N. Holben, M. D. King, S. C. Tsay, E. M. Prins, D. E. Ward, K. M. Longo, L. F. Mattos, C. A. Nobre, J. D. Spinhirne, A. M. Thompson, J. F. Gleason, and S. A. Christopher, 1998: The Smoke, Clouds and Radiation Experiment in Brazil (SCAR-B). *J. Geophys. Res*., submitted.

4. Kaufman, Y. J., R. Kleidman, M. D. King and D. E. Ward, 1998: SCAR-B fires in the tropics: Properties and their remote sensing from EOS-MODIS. *J. Geophys. Res*., submitted.

5. Kaufman, Y. J., D. Tanré, H. R. Gordon, T. Nakajima, J. Lenoble, R. Frouin, H. Grassl, B. M. Herman, M. D. King and P. M. Teillet, 1997: Passive remote sensing of tropospheric aerosol and atmospheric correction for the aerosol effect. *J. Geophys. Res*., **102**, 16815–16830.

6. King, M. D., Y. J. Kaufman, D. Tanré and T. Nakajima, 1998: Remote sensing of tropospheric aerosols from space: Past, present, and future. *Bull. Amer. Meteor. Soc*., in preparation.

7. King, M. D., S. C. Tsay and S. A. Ackerman, 1997: MODIS Airborne Simulator: Radiative properties of smoke and clouds during ARMCAS and SCAR-B. *Proc. Third International Airborne Remote Sensing Conference and Exhibition*, Copenhagen, Denmark.

8. King, M. D., S. C. Tsay, S. A. Ackerman and N. F. Larsen, 1998: Discriminating heavy aerosol, clouds, and fires during SCAR-B: Application of airborne multispectral MAS Data. *J. Geophys. Res*., submitted.

9. King, M. D., S. C. Tsay, S. E. Platnick, M. Wang and K. N. Liou, 1997: Cloud Retrieval Algorithms for MODIS: Optical Thickness, Effective Particle Radius, and Thermodynamic Phase, *MODIS Sci. Team Rep.*, ATBD-MOD-05, 79 pp.

10. Li, J. Y., H. G. Meyer, G. T. Arnold, S. C. Tsay, and M. D. King, 1997: *The Cloud Absorption Radiometer HDF Data User's Guide*. NASA Technical Memorandum 104643, 34 pp.

11. Platnick, S., P. A. Durkee, K. Nielson, J. P. Taylor, S. C. Tsay, M. D. King, R. J. Ferek, P. V. Hobbs and J. W. Rottman, 1998: The role of background cloud microphysics in the radiative formation of ship tracks. *J. Atmos. Sci*., in press.

12. Soulen, P. F., R. Pincus, S. C. Tsay and M. D. King, 1997: Cloud Absorption Radiometer: Airborne measurements of clouds and surface reflectance. *Proc. Third International Airborne Remote Sensing Conference and Exhibition*, Copenhagen, Denmark.

13. Tsay, S. C., M. D. King, G. T. Arnold and J. Y. Li, 1998: Airborne spectral measurements of surface anisotropy during SCAR-B. *J. Geophys. Res*., in press.

14. Wang, M., and M. D. King, 1997: Correction of Rayleigh scattering effects in cloud optical thickness retrievals. *J. Geophys. Res*., **102**, 25,915–25,926.